International Forum on Aeroelasticity and Structural Dynamics
IFASD 2024
17-21 June 2024, The Hague, The Netherlands

WIND TUNNEL FLUTTER TEST RESULTS COMPARISON WITH COMPUTATIONAL RESULTS OF A HALF-SPAN WING

Amanda P. Perroni[1], Breno M. Castro[1], Eduardo P. Krupa[1], Manoela S.C. Lima[1], Marlus R.B. Kerninski[1], Michelle F. Westin[1*], Jens Neumann 2[2]

[1] Embraer S.A., Av. Brigadeiro Faria Lima, 2170, zip code: 12.227-901, Sao Jose dos Campos, Brazil
[2] German Aerospace Center (DLR), Institute of Aeroelasticity, 37073 Göttingen, Germany

Keywords: transonic regime, CFD/CSM-methods, flutter, wind tunnel experiment

Abstract: A half-span wing was designed for wind tunnel test for verification of aeroelastic characteristics in 2017. This wing was quite flexible and fitted with a pylon and a flow thru nacelle, to represent the geometry and mass distribution of real-life aircraft, but without propulsion effects, see Fig.1.

The wind tunnel used in 2017 for aeroelastic tests was the DNW-HST in Amsterdam, The Netherlands. The test was split in two parts: the first campaign focused on wing deflection for each test point and on how the flexibility affected the flutter characteristics. The second part was dedicated to higher Mach numbers and low angles of attack to verify the effect of both flexibility and shock waves on the aeroelastic characteristics of the system. The wind tunnel test instrumentation included steady and unsteady pressure taps, accelerometers, strain gauges, stereo pattern recognition, and others.

All wind tunnel measurements were in good agreement to the computational results, obtained by using traditional tools, such as Nastran. However, for the second entry, considering Mach numbers from 0.75 to 0.90, the behaviour of both damping and frequency are slightly different from the computational analysis, especially for the first five aeroelastic modes. The results were obtained for three different configurations by varying the wing tip mass.

Since there are some differences between the experimental and computational results for the transonic regime, further analysis is performed to explore the effects of aerodynamic nonlinearities. To investigate it in more detail, analyses using different computational tools for the transonic unsteady aerodynamics from Embraer and DLR is used in the present paper and compared with the experimental results obtained in 2017. The focus is to use high fidelity methodologies based on coupled CFD/CSM-methods (computational fluid dynamics, computational structure mechanics) for the flexible model to better capture nonlinear phenomena that might be occurring during the wind tunnel tests.

1 INTRODUCTION

Aeroelastic solutions are constantly evolving to capture nonlinearities of different natures, such as aerodynamic, structural, and geometric. Considering the analysis methodology improvement to better characterize and understand nonlinear aeroelasticity, Embraer and DLR (German Aerospace Center) have developed a wind tunnel model highly flexible, so structural nonlinearities are present and have influence in the aeroelastic behavior of the model shown in Fig. 1.

It is well known that flutter is a phenomenon to be avoided for the entire aircraft envelope and methodologies to predict flutter velocity and frequency are well stablished. However, for nonlinear cases, the current methodologies shall be modified to incorporate this sort of effect. For the case under evaluation, the flutter analysis shall consider high structural flexibility.

The model is a generic wing, with pylon and nacelle under it. The half fuselage is rigid and has no influence on the overall flutter behavior. Only the wing is highly flexible. This model is not representative of any actual aircraft and was used for these wind tunnel tests purely for technological development. This model was designed in 2015 and 2016, by NLR (Netherlands Aerospace Center), and tested in HST (high speed tunnel) in 2017. HST is a wind tunnel located in Amsterdam, The Netherlands, as part of DNW consortium (German-Dutch Wind Tunnels).

The wind tunnel model was heavily instrumented with dynamic pressure transducers, accelerometers, strain gauges, stereo pattern recognition, etc. There were two different tests campaigns: the first was for lower speeds, up to Mach number 0.70, but achieving high angles of attack, focusing on wing high deformation. The second entry was focused on higher velocities, from Mach number 0.75 to 0.90, but lower angles of attack. In this second entry, besides the high level of deformation expected for this wing, the presence of shock waves is also noted. For this reason, CFD-based (computational fluid dynamics) methodologies might present higher fidelity results, hence, closer to the results expected from flight tests.

Nevertheless, the idea of this paper is to use two different CFD-based tools, DLR-TAU and AERO coupled with NASTRAN to compare with the wind tunnel results. The differences between them shall be discussed later.

For this reason, this paper is organized as follows. A brief description of the wind tunnel (WT) model design strategy, manufacturing and testing is provided in Section 2. Section 3 introduces the different finite-element models, CFD meshes, CFD solvers, and fluid-structure methodologies used by Embraer and DLR to pursue high-fidelity steady aeroelastic analyses and estimate the model flutter boundary. The main simulation cases studied are presented in Section 4 along with the results discussion. It addresses comparisons regarding pressure distributions (and the resulting lift coefficients), as well as flutter velocity-frequency-damping (v-f-g) plots. Lastly, concluding remarks are drawn in Section 5.

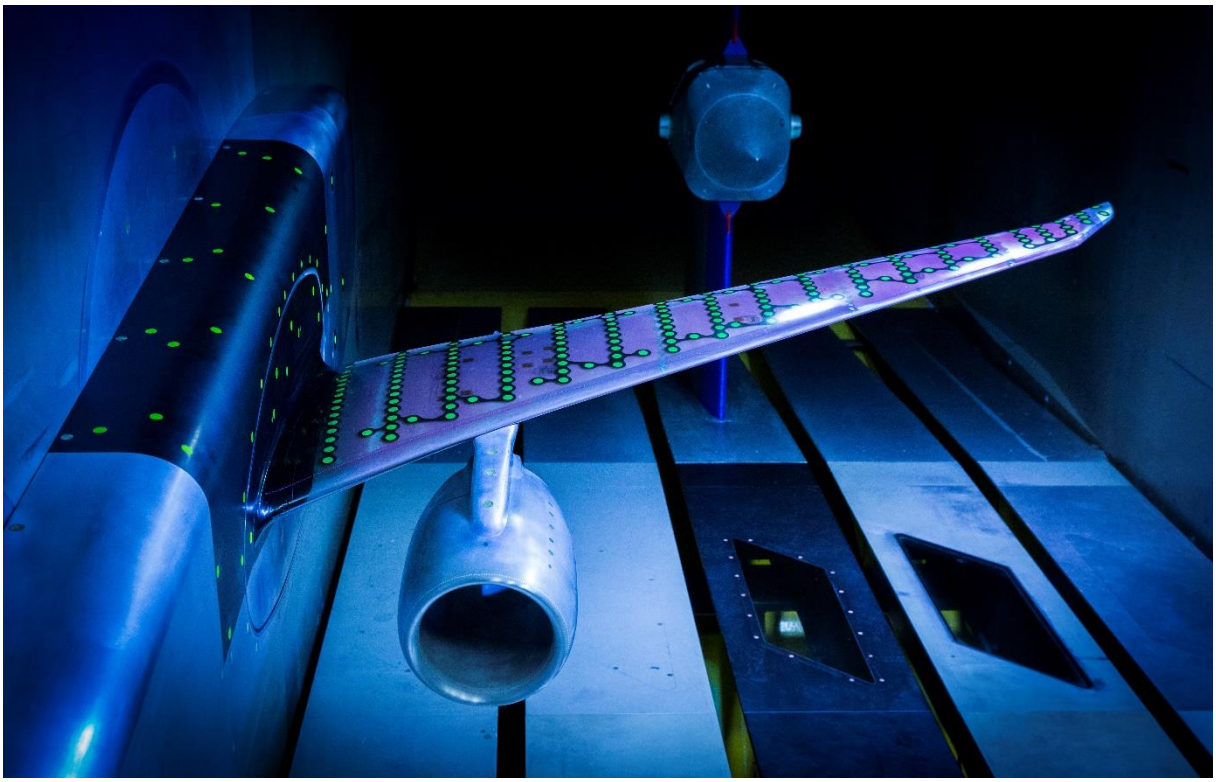

Figure 1: Transport aircraft wing model mounted in DNW-HST.

2 WIND TUNEL MODEL DESIGN AND TESTING

This section aims to briefly describe the wind tunnel model and how the test proceeded. Since there are other dedicated publications on these subjects, this section is not supposed to bring details, only general information.

2.1 Model Design Methodology

To design the model, the goals of the test shall be specified. In this case, a very flexible wing was designed and built to validated more efficient numerical methodologies and processes to predict flutter at Embraer considering the following scenario: very high deformations, transonic Mach numbers (to 0.4 to 0.9), different angles of attack and different stagnation pressures. In this case, the experiment investigated the nonlinearity due to high deformation, that is, high structural displacements.

Since the design of wings subjected to such nonlinear effects is very important in the experiment safety aspect, to predict the wing bending and torsion modes properly, considering aerodynamic nonlinearities due to shock waves, is crucial for the test success. All the design process can be found in more detail in [1].

For the design of the wind tunnel model, the first step is the pre-design phase. In this phase, it is necessary to understand if the required flexibility is feasible. To this end, the DLR-AE (Institute of Aeroelasticity in DLR) developed a process to optimize the aeroelastic stiffness. For this optimization, both Nastran and DLR-AE in-house tool Modgen were used in the pre-design stage [1].

The pre-design optimization process used an aeroelastic tailoring approach and was based on the stiffness of the wing model and some lamination parameters. The optimization function to be maximized was the wing tip deflection. The load carrying skin made of fiberglass and a foam core supporting the skin and preventing buckling and compression loads compose the wing structure. The optimization scheme considered the following wing sections along the span, like shown in Fig. 2.

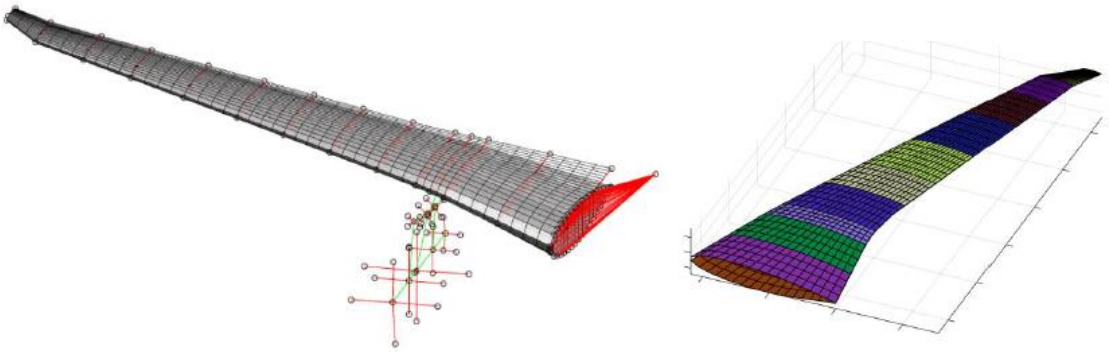

Figure 2: Finite element model (left) and wing sections for optimization (right) [1].

With the deformed wing, the CFD mesh is updated, and new loads are obtained (Fig. 3).

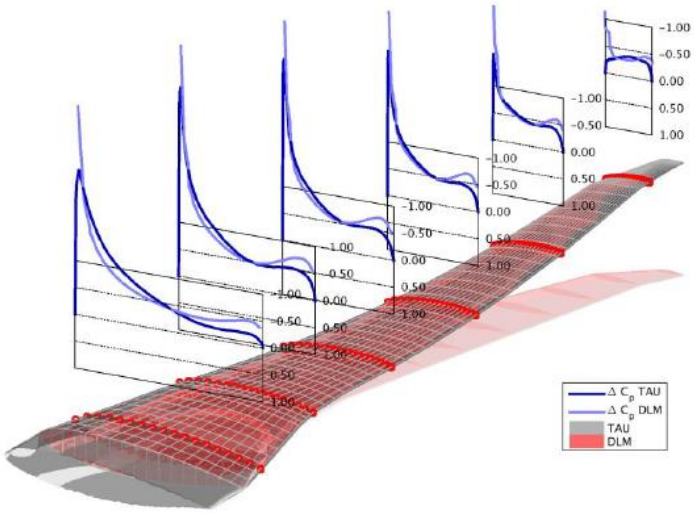

Figure 3: Wing deformation with updated mesh and wing loads [1].

After the model's conception using the optimization process, the detailed design model shall be done. First, the detailed computational finite element model (FEM) is done using Abaqus (Fig.4), which is used to generate the mass and stiffness matrices to be input later in MSC Nastran. MSC Nastran is used for both modal analysis and aeroelastic analysis. More information about the detailed design can be found in [2].

Regarding the boundary conditions, during the development of the structural dynamic (FEM), a high-fidelity boundary condition was modeled considering the wind tunnel interface with the model, like represented in Fig. 5. This modeling is necessary to represent the flutter behavior as accurately as possible [2].

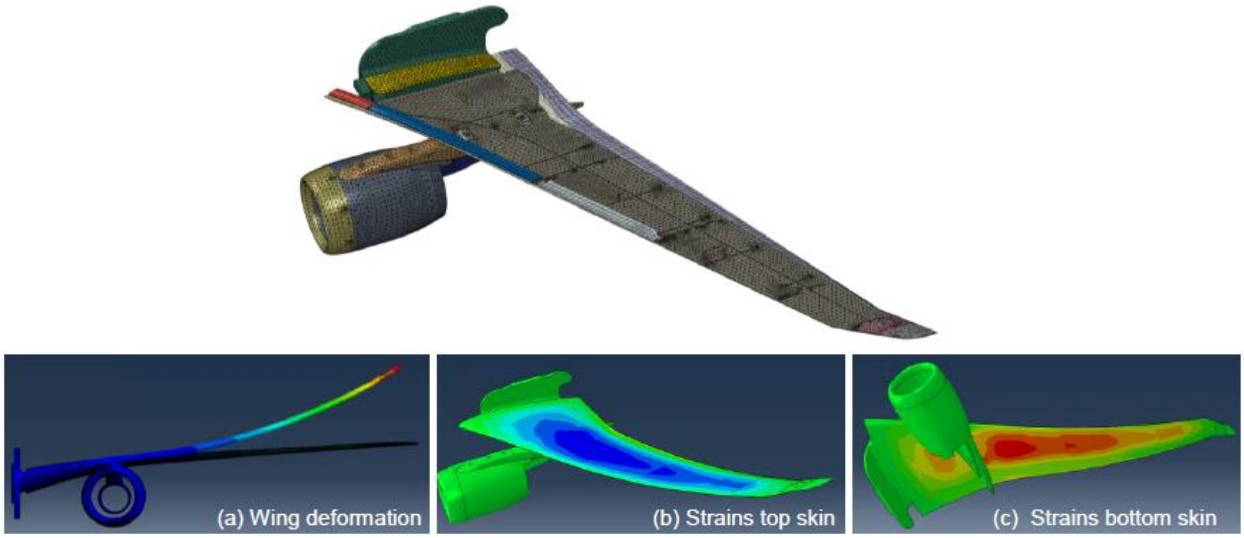

Figure 4: Detailed FEM (top) and structural analysis (bottom) [1].

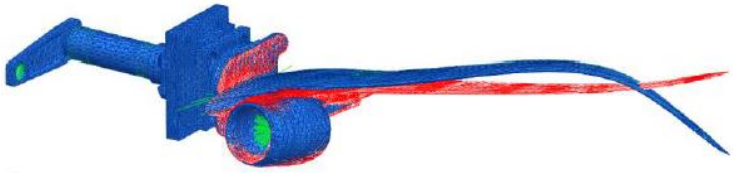

Figure 5: Detailed FEM with high-fidelity boundary condition [2].

2.2 Model Manufacturing

The model was manufactured using different materials for each part. Considering the wing and to enable its high deflections as required, it was made of glass fiber reinforced plastic (GFRP), which exhibit linear behavior up to very high strain levels. The lay-ups are defined during the pre-design phase, like shown in Fig. 2. Like exposed in 2.1, the wing core is made of foam (Rohacell) to prevent buckling and compression loads. The other parts of the wing are: fillet (aluminum), tip (aluminum with tungsten used to vary the wing tip mass), root (steel), fuselage/fairing (aluminum), pylon (aluminum and magnesium) and nacelle (aluminum and magnesium). The final assembly is shown in Fig. 6 and Fig. 1 (inside the wind tunnel test section). About the model manufacturing it can be found in [1].

Figure 6: Assembled model outside the wind tunnel section (left) [1].

2.3 Wing Tunnel Testing

This section's objective is to present some overall information about the wind tunnel tests. For more information and deeper analysis, other previous publications will be referred.

2.3.1 Wind tunnel facility

The wind tunnel used for the tests was the DNW-HST, which is the high-speed tunnel in the German-Dutch Wind Tunnels consortium, located in Amsterdam, The Netherlands.

The test section is a closed loop 2.0m wide by 1.6m or 1.8m height and its Mach numbers goes from 0.15 to 1.35. There is a compressed air supply with capacity of 8kg/s at 40 bar and the model was sided wall supported, like shown in Fig.1. All information about DNW wind tunnels and specifically about HST can be found in [3].

2.3.2 Bench tests and model calibration

To validate the finite element model after the design and manufacturing phases, a GVT (ground vibration test) is necessary. In fact, the model calibration could be split into four steps: initial GVT, static load and high deflection test, calibration of the strain gauges and GVT verification.

The objective of the initial GVT is to update the FEM, providing information of the manufactured model to the computational model to match the first five modes, regarding mode shape and frequencies. The static load and high deflection test objective are to test the model for the worst load case and verify if the model is prepared for the wind tunnel test without failure (Fig. 7). The calibration of strain gauges provides a conversion matrix for sectional loads presentation. With all these tests results, the final GVT can be performed again, following the same methodology as the

first GVT and with the idea of updating the model again, if necessary. The GVT is done again because the model was subjected to very high loads and deflections that might cause a difference from the previous results, so it is necessary to check again.

For better model characterization, the GVT of the model was performed in laboratory and with free-free (Fig. 8) and clamped (Fig. 9) boundary conditions. Also, the GVT was performed with and without the pylon-nacelle set. The pylon-nacelle set was tested individually in different clamped dispositive (Fig. 9). Before starting the wind tunnel test, a GVT was also performed into the wind tunnel test section (Fig.10).

Figure 7: Load and deflection test (LAD is the load application device) [2].

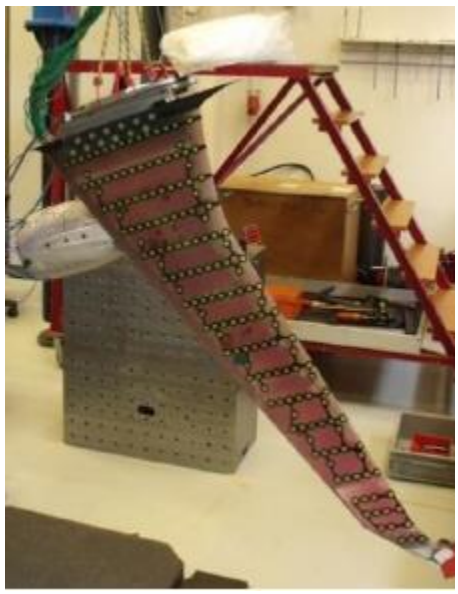

Figure 8: Model GVT in free-free condition [2].

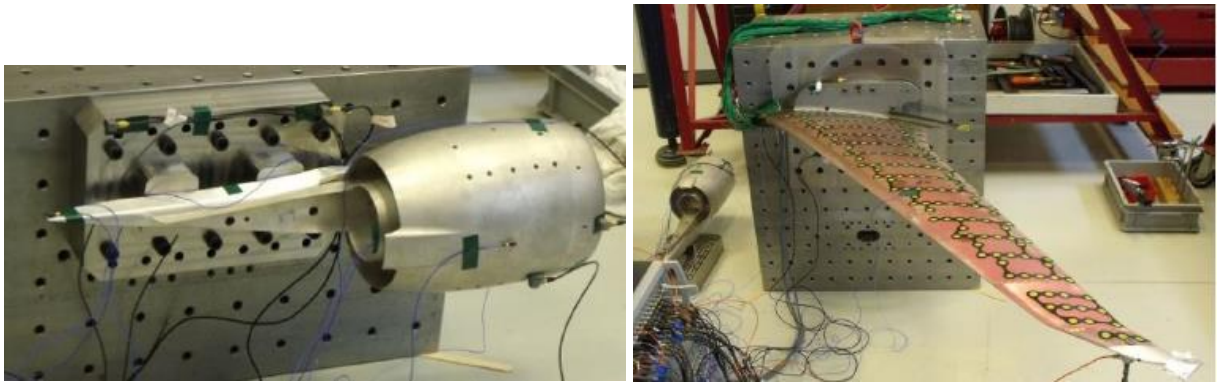

Figure 9: Pylon-nacelle (left) and wing (right) GVT [2].

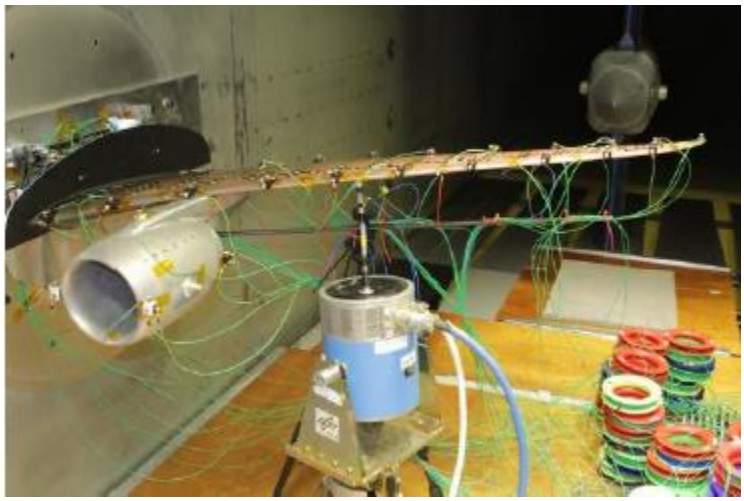

Figure 10: GVT inside the wind tunnel test section [2].

After these ground tests, the FEM is updated, like shown in more details in [2]. This correlation is obtained using modal assurance criterion (MAC).

2.3.3 Load signals and online modal analysis

As shown in Fig. 1, the model is attached to the wind tunnel side wall at a turntable to be possible to change the angle of attack for each matrix point. In this paper, only 0° will be considered for the analysis and for brevity. The data acquisition system used during the tests depended on the data to be acquired. For steady signals, the standard data acquisition system available in HST was used combined with optical systems. For unsteady signals, two independent data acquisition systems were used. For time signals, there were piezoelectric balance, accelerometers, strain gauge bridges, laser distance measurement devices and servo valve control signal. To access the flutter stability online, parallel acceleration, strain gauge signals, forces from piezoelectric balance and wind tunnel parameters were acquired in a dedicated online system. For more details about the measurement set up, refer to [1].

To guarantee the safety of the test, an online monitoring system was developed, based on output-only operational modal analysis. Due to the risk of failure of the model during the test, a fast and

reliable identification of eigenfrequencies and damping ratios using continuous operational modal analysis was applied for this test and a system was developed [4]. The method is based on the continuous application of an output-only modal analysis, applied to acceleration responses of the model. The excitation, in this case, is provided by the natural turbulence of the incoming flow during the test. More detailed information about this system and the formulation used to design it can be found in [4].

3 METHODOLOGY

This section describes the different approaches employed by Embraer and DLR to investigate the HMAE WT results for Mach numbers beyond 0.75 and up to 0.84 (higher Mach numbers -up to 0.90 - will be investigated numerically in a future study). Each one has adopted a distinct research strategy (CFD and FE models, solvers, and flutter calculation approach) that aligns with their specific knowledge, established best practices, and resources available, resulting in more diverse perspectives on the same research problem. The results comparisons presented within this work also intend to understand how these various techniques can be applied to the same problem and what potential insights each methodology may yield.

3.1 Finite Element Model

The finite element model used both by DLR and Embraer is the same as the one created by NLR and applied at DLR, shown in Figure 5. The reader is referred to Ref. [2] for a more detailed description of the model.

3.2 Aerodynamic Model

The choice of the aerodynamic models was based on factors related to computational efficiency and ease of handling the aeroelastic coupling and boundary layer modeling. For the CFD models, Embraer and DLR used very similar surface meshes of the Wing-Body-Pylon-Nacelle (WBPN) but different in their approaches to modeling the boundary layer (BL) for the RANS computations. While DLR's model was provided by Embraer and used 50 prismatic layers for the BL in their volumetric mesh, Embraer did not use the same approach, employing a wall function instead.

Some of the benefits of using prismatic layers include a more representative modeling of the flow physics near the wall, better capturing the behavior of laminar-turbulent transitional regions. However, this modeling approach leads to increased computational cost and additional difficulties in updating the displacements in the FSI iterations, often causing problems of negative volumes or mesh crossovers. Contrary to that, wall function methods (with fewer prismatic layers or none – like a Euler mesh), offers lower computational wall times and simpler aeroelastic coupling (surface and volume mesh deformation to update the pseudo-iterations displacements) at the expense of lower accuracy near walls for turbulent flows. These accuracy issues may become more relevant as the flow becomes more non-linear (i.e., higher Mach numbers or greater displacements). Figure 11 depicts details of the HMAE – WBPN CFD mesh.

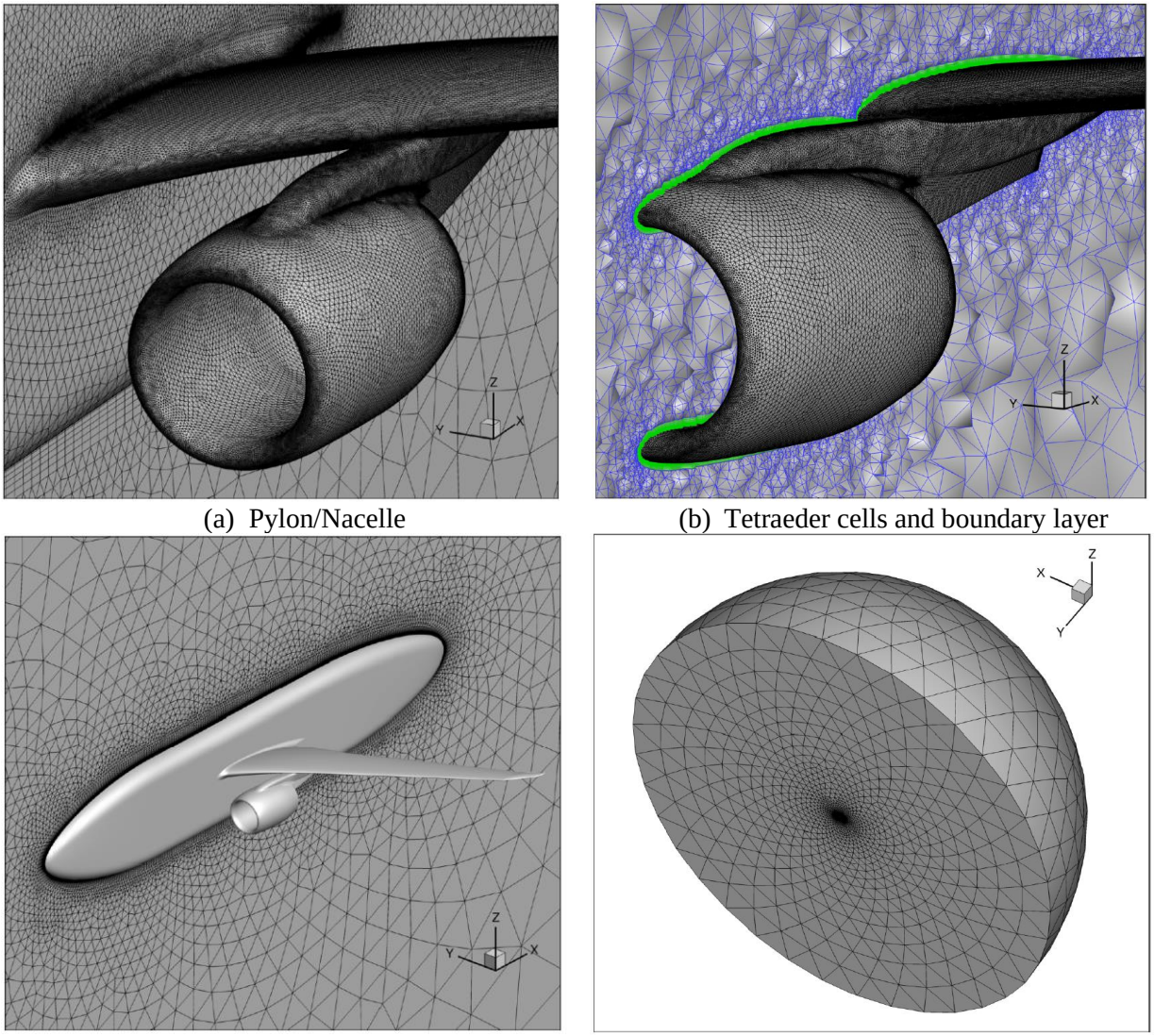

(a) Pylon/Nacelle (b) Tetraeder cells and boundary layer

(c) WT model and symmetry plane (d) Farfield

Figure 11: Details of the CFD mesh of the HMAE WT model (with prismatic layers for the volume mesh).

3.3 CFD Solvers

*3.3.1 **AERO CMSoft, inc:***

The AERO-Suite is a multidisciplinary commercial package developed by CMSoft, Inc [5] especially designed for high-fidelity aeroelastic analysis. Amongst the AERO available solutions, the most relevant for the aeroelastic analysis pursed in this work, includes high-fidelity steady FSI solutions, and the construction of generalized aerodynamic matrices (GAM). The Embraer's aerodynamic analyses are carried out with the AERO-F module of AERO Suite. It works as a 3D compressible Euler/Navier-Stokes solver featuring several turbulence modeling capabilities. All the simulations presented here were performed using 3D RANS equations with the wall-function to speed up the FSI aeroelastic sub-iterations. The turbulence model employed was the by the well-known Spalart-Almaras [6] model. The Generalized Minimum Residual (GMRES) solver with 80

Krylov vectors is used to solve both the Navier-Stokes equations and the turbulence equations. The volume mesh partitioned into 240 domains and the simulations are run in parallel to achieve lower computational walltimes.

3.3.2 TAU solver:

The DLR's computation of the aerodynamic loads involves solving the 3D RANS equations with the DLT-TAU code [7]. To perform a spatial discretization, a central scheme featuring a central scheme was used along with an implicit lower-upper symmetric Gauss-Seidel (LUSGS) iteration scheme. Flow turbulence is also addressed by the Spalart-Almaras model. All the simulations were executed in parallel using a single grid technique with the volume mesh partitioned into 240 domains to achieve lower computational walltimes.

3.4 Fluid-Structure Interaction (FSI)

3.4.1 Spatial Coupling:

For the FSI calculations, DLR's approach for the spatial coupling, that is, the loads and displacements transfer between the non-matching CFD and FE models, is centered around the construction of linear operator H. This operator is used to map the displacement field from the FE model onto the CFD surface mesh, such that:

$$\Phi_{\mathrm{CFD}} = H\Phi_{\mathrm{FE}} \tag{1}$$

In Eq. (1), Φ_{FE} is the modal basis in the FE grid domain, whereas Φ_{CFD} is the modal basis in the CFD surface mesh domain. The calculation of the matrix H is done using a radial basis functions approach [8]. It is worth mentioning that care was taken to guarantee that the displacements of the fixed surfaces (i.e. body surface) were always zero for every mode shape.

The spatial coupling used along with the AERO software is based on the pre-processing module named Matcher [5]. The Matcher module provides an option to use an intermediate mesh to interface the non-matching CFD and FE models. This intermediate mesh is often called a "phantom mesh" and produces a "dress model" FE. The phantom mesh is a much coarser CFD mesh that represents sufficiently well the outer mold line of the model with a mesh resolution of the same order of that of the FE model.

The Matcher will then create the dress model by converting the phantom mesh elements into structural shell elements (without stiffness) and connect then to the original FE grids with rigid bars. The output is a FE model with a geometric representation more closely related to that of the CFD surface mesh. It was found that this approach improves the convergence of steady aeroelastic simulations better handling the modal shapes. Figure 12 illustrates the phantom mesh used throughout this work.

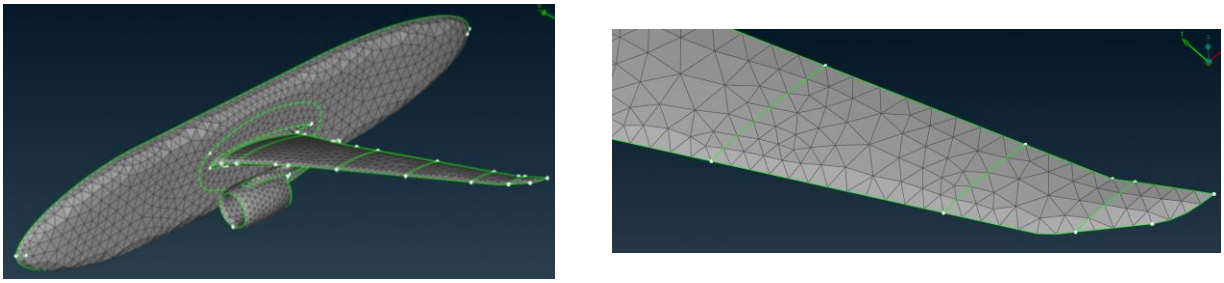

Figure 12: Phantom mesh used in the AERO simulations.

3.4.2 FSI Solution Procedure:

Both approaches of DLR and Embraer to solve the steady state aeroelastic problem are based on a modalized representation of the structure. In particular, DLR formulates the FSI problem as in:

$$\Omega q - Q(q) = 0 \tag{2}$$

In Eq. 2, q denotes the modal deformation state, Ω is the diagonal matrix of the squared modal stiffnesses and Q represents the generalized aerodynamic forces. It is worth mentioning that Q is a projection of the nodal aerodynamic forces (f_{CFD}) onto the modal basis as defined in the aerodynamic surface mesh, such that:

$$Q = \Phi_{\mathrm{CFD}}^{T} f_{\mathrm{CFD}} \tag{3}$$

The modal deformation state of the iteration *n+1* is obtained according to:

$$q_{n+1} = \Omega^{-1} Q(q_n) \tag{4}$$

The FSI solution is achieved within 3-10 iterations and is said to be converged when the tip displacement is within a tolerance of 1 mm. The aerodynamic surface deformation in cartesian coordinates is recovered following the relation:

$$\mathrm{x}_{\mathrm{CFD}} = \Phi_{\mathrm{CFD}} q \tag{5}$$

This deformation is then propagated to the volume mesh via an advancing front algorithm.

Embraer's approach to solve the FSI problem lies in the solution available in the software AERO named *"Steady Aeroelastic (Modalized Structure)"*. To perform a Steady aeroelastic analysis using this solution, the AERO fluid solver (known as AERO-F) requires that the structure be represented by a truncated subset of its mode shapes, and therefore the structure is assumed to have a linear behavior.

As will be explained in more detail in later sections, this modal basis is obtained using Nastran SOL103, normalized by mass, and translated into AERO's format. To ease the convergence (especially for the higher Mach numbers), a steady-state solution of the undeformed wing (rigid) is used as an initial solution of the FSI problem as implemented in AERO. Additionally, an under-relaxation factor per global pseudo-iteration is also used to control the coupling strength/stability by moderating the displacements updates between the iterations.

3.5 Flutter Analysis

This section describes the step-by-step procedure used to calculate flutter by importing the generalized aerodynamic matrix QHH as output by AERO into the Nastran Solution 145. Note that the QHH matrix is a function of the Mach number and the reduced frequency and is calculated in Nastran by means of linear low-fidelity methods (the well-known Doublet Lattice Method – DLM). The approach described next intends to use a high-fidelity QHH calculated with an external aerodynamic solver (in this case, AERO) and augment the Nastran flutter calculation. The procedure is as follows:

Step 1 - Modal Analysis: The first step is to perform a modal analysis using Nastran SOL103, which generates the modal basis of the structural dynamic model. For the analyses presented

throughout this study, the first 20 modes were used (all flexible modes since the structure is clamped at the root).

Step 2 - Data translation: Using in-house (Embraer) scripts, this Nastran modal basis is translated into a format compatible with CMSoft AERO's input requirements (both file format and coordinate system).

Step 3 - Basis Ping-Pong: In this step, a simulation known in AERO as the Basis Ping-Pong (BPP) is performed. In the BPP procedure, the structural AERO solver (known as AERO-S) sends to the AERO fluid solver (AERO-F) the user-specified displacement fields, in this case, modal displacements. The AERO-F then transfers this data to the CFD mesh adapting its grids for each mode shape of interest. The BPP step provides "sources of excitation" for the QHH calculation, as addressed in a later step.

Step 4 - Steady CFD Simulation: Next, for each of the WT runs studied here, a steady CFD simulation is carried out with the aerodynamic shape assumed to be rigid (CFD only – the structural solver is not used in this step). The solution is assumed converged when the flow equations residual achieves an order of 1.0e-7. This converged solution is then used as an initial flow state for the FSI procedure. It was found that using the steady solution as a restart for the FSI calculation effectively improves the FSI analysis leading to lower wall times and more robust convergence.

Step 5 - FSI Procedure: For the same flight conditions used in Step 4, a steady-state aeroelastic calculation is performed. The spatial coupling and FSI procedure used in this step is described in Section 3.4.

Step 6 – High-Fidelity QHH: For each Mach number and reduced frequency pair of interest, a generalized aerodynamic matrix (GAM or QHH as in Nastran) is calculated using a feature available in AERO named "*GAMConstruction*" using the modal basis calculated in Step 3 and the linearized around the flow/position equilibrium solution obtained in Step 5.

Step 7 - Nastran Solution 145 augmented with a high-fidelity QHH: Finally, the high-fidelity QHH calculated in Step 6, is fed into the Nastran SOL145 with proper DMAP ALTERS. Flutter is then performed using the PKNL method.

4 RESULTS DISCUSSION

The WT runs and FSI simulations covered a wide range of Mach numbers ($0.75 < M < 0.90$), dynamic pressures ($25 < Q < 55\,kPa$) and angles of attack ($-2.0 < AoA < 0.0$ deg). However, for reasons of brevity, only results of the cases shown in Table 1 will be addressed. The chosen cases are representative of the broader wind tunnel test matrix and overall analyses trends observed in the research. The results presented in this section will cover pressure coefficients, and flutter v-g-f curves.

Case number	Simulation name	Mach	Re [1.0e6]	Alpha [deg]	Approx. Q [kPa]
1	HMAE-16-02-173-M75-25-SA	0.75	3.4	0.0	25
2	HMAE-19-02-215-M78-25-SA	0.78	3.3	0.0	25
3	HMAE-19-03-218-M80-25-SA	0.80	3.2	0.0	25
4	HMAE-20-01-224-M82-25-SA	0.82	3.2	0.0	25
5	HMAE-20-02-227-M84-25-SA	0.84	3.1	0.0	25
6	HMAE-18-05-206-M75-55-SA	0.75	7.2	0.0	55
7	HMAE-32-06-430-M78-55-SA	0.78	7.0	0.0	55

8	HMAE-24-06-293-M80-55-SA	0.80	6.8	0.0	55
9	HMAE-26-02-315-M82-55-SA	0.82	6.8	0.0	55
10	HMAE-27-04-345-M84-55-SA	0.84	6.6	0.0	55

Table 1: Summary of WT-runs investigated in this work.

4.1 Pressure Coefficients

Pressure coefficient results for numerical and experimental data are shown in Figure 13 through Figure 22 for the span stations of η=65% and 84%.

The pressure coefficients obtained with AERO (RANS simulations with wall functions), overall, showed a good agreement with the wind tunnel data for most of the chordwise extension of the upper and lower parts and for Mach numbers up to 0.84. It is noted, however, that, for all cases, there was a minor difference in pressures along the upper region which exhibited stronger shocks than the experimental, and TAU full RANS (no wall function) counterpart results.

Furthermore, in the simulations that used wall function, the pressure coefficients were found to be more consistent with the experimental data for the higher Reynolds numbers ($Re > 6.0$), whereas for the lower dynamic pressures and high Mach numbers (cases 4 and 5 - $Re \approx 3.0$), the shocks strength was also over predicted. These differences are expected due to the limitations of the wall function method in not fully capturing shock-boundary-layer interactions. Nonetheless, regardless of these deficiencies, it is thought that the results obtained using wall functions could be used as a good starting point solution for the more expensive FSI RANS computations with CFD meshes featuring Y+ close to 1. Overall, full RANS solutions showed a closer agreement with the experimental data correctly predicting the shock strength though higher wall times were achieved.

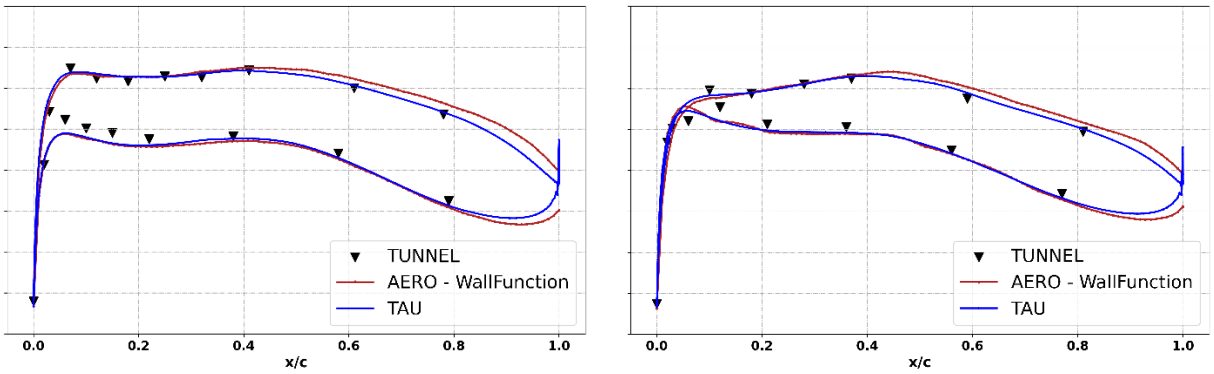

Figure 13: Comparison of simulated Cp distributions at spanwise stations η=65% (left) *and* 84% (right) - polar *HMAE-16-02-173-M75-25-SA*, Mach 0.75, alpha =0 deg, Q=25kPa.

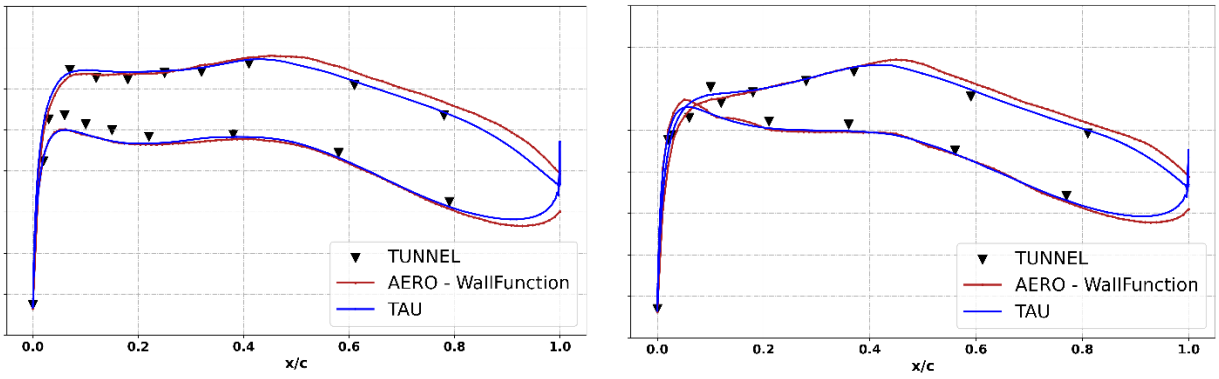

Figure 14: Comparison of simulated Cp distributions at spanwise stations η=65% (left) *and* 84% (right) - polar *HMAE-19-02-215-M78-25-SA*, Mach 0.78, alpha =0 deg, Q=25kPa.

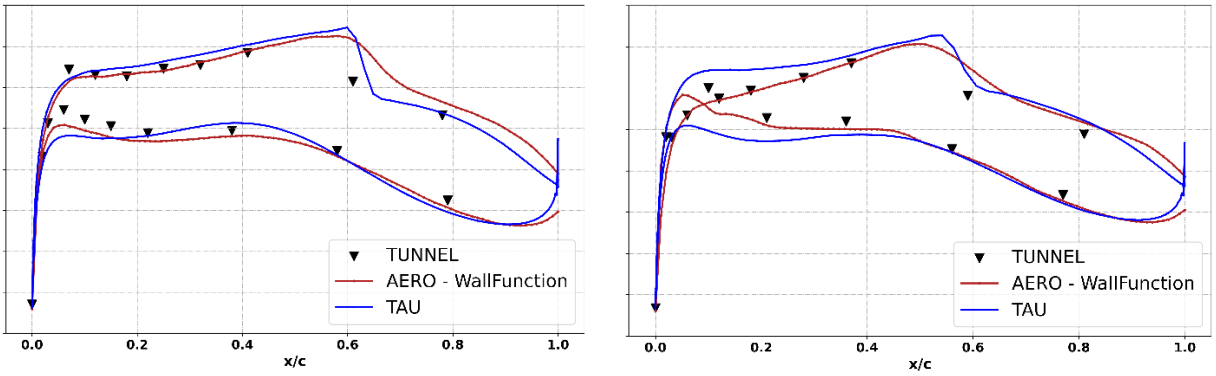

Figure 15: Comparison of simulated Cp distributions at spanwise stations η=65% *(left)* and 84% *(right)* - polar *HMAE-19-03-218-M80-25-SA*, Mach 0.80, alpha =0 deg, Q=25kPa.

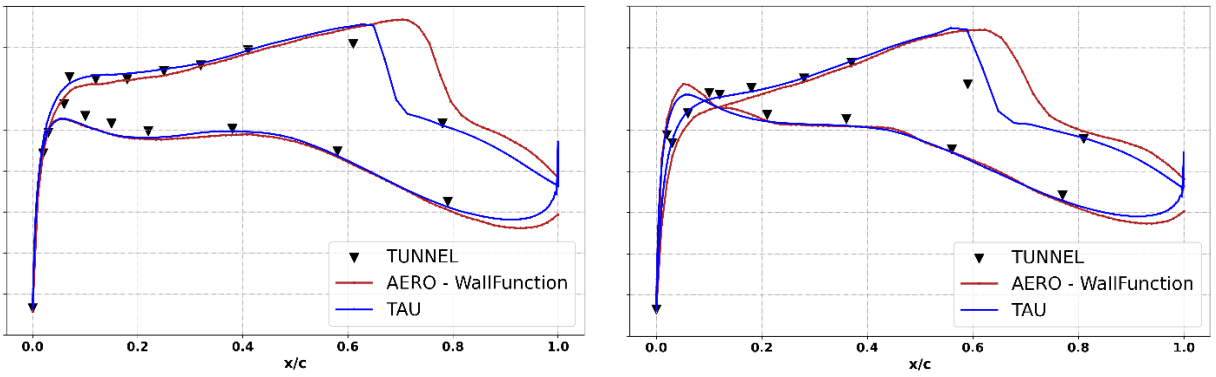

Figure 16: Comparison of simulated Cp distributions at spanwise stations η=65% (left) *and* 84% (right) - polar *HMAE-20-01-224-M82-25-SA*, Mach 0.82, alpha =0 deg, Q=25kPa.

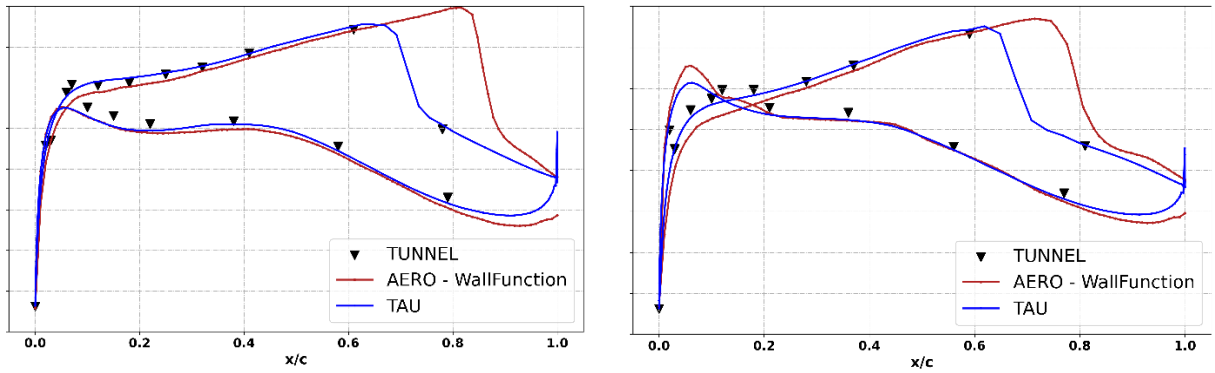

Figure 17: Comparison of simulated Cp distributions at spanwise stations η=65% (left) *and* 84% (right) - polar *HMAE-20-02-227-M84-25-SA*, Mach 0.84, alpha =0 deg, Q=25kPa.

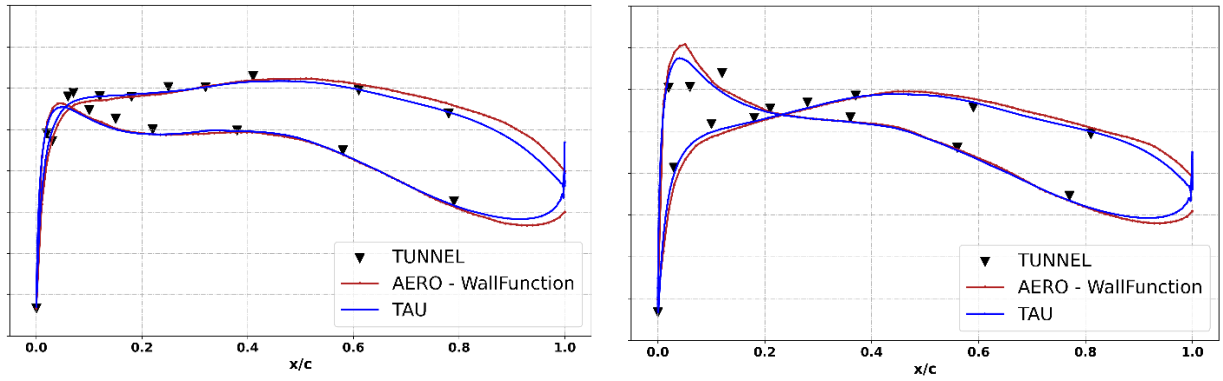

Figure 18: Comparison of simulated Cp distributions at spanwise stations η=65% (left) *and* 84% (right) - polar *HMAE-18-05-206-M75-55-SA*, Mach 0.75, alpha =0 deg, Q=55kPa.

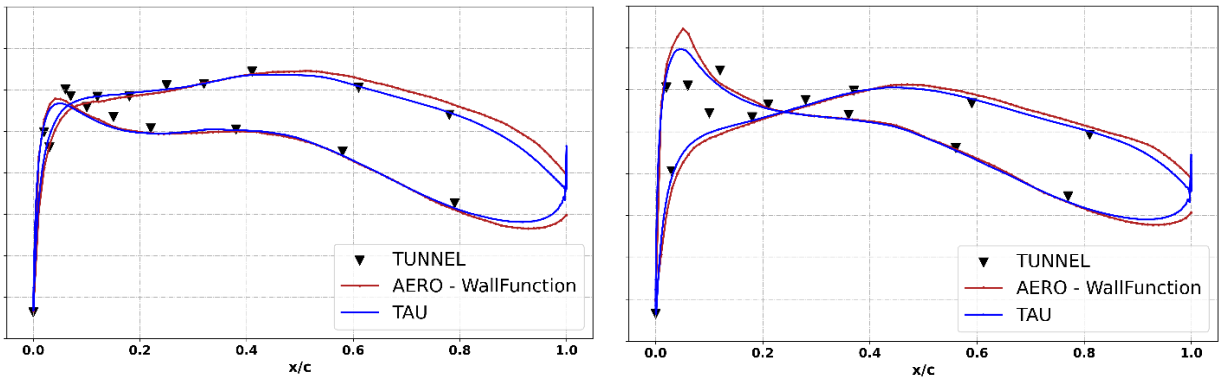

Figure 19: Comparison of simulated Cp distributions at spanwise stations η=65% (left) *and* 84% (right) - polar *HMAE-32-06-430-M78-55-SA*, Mach 0.78, alpha =0 deg, Q=55kPa.

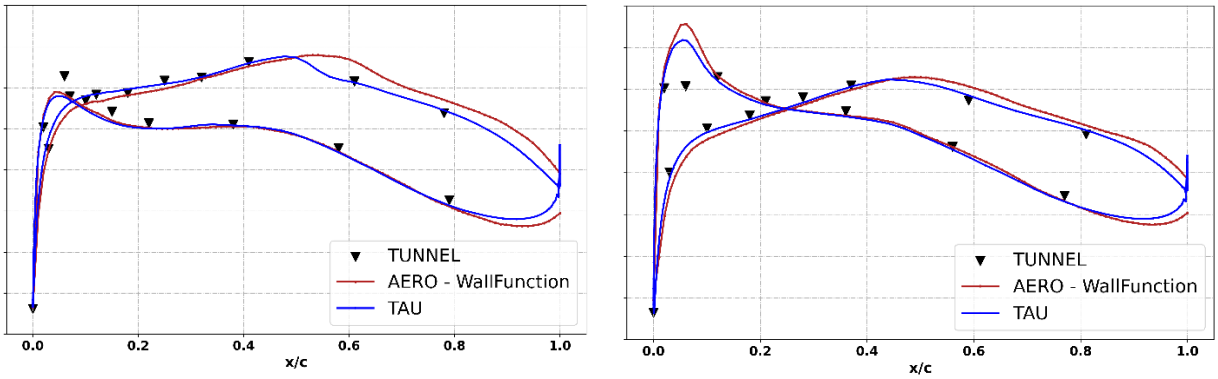

Figure 20: Comparison of simulated Cp distributions at spanwise stations η=65% (left) *and* 84% (right) - polar *HMAE-24-06-293-M80-55-SA*, Mach 0.80, alpha =0 deg, Q=55kPa.

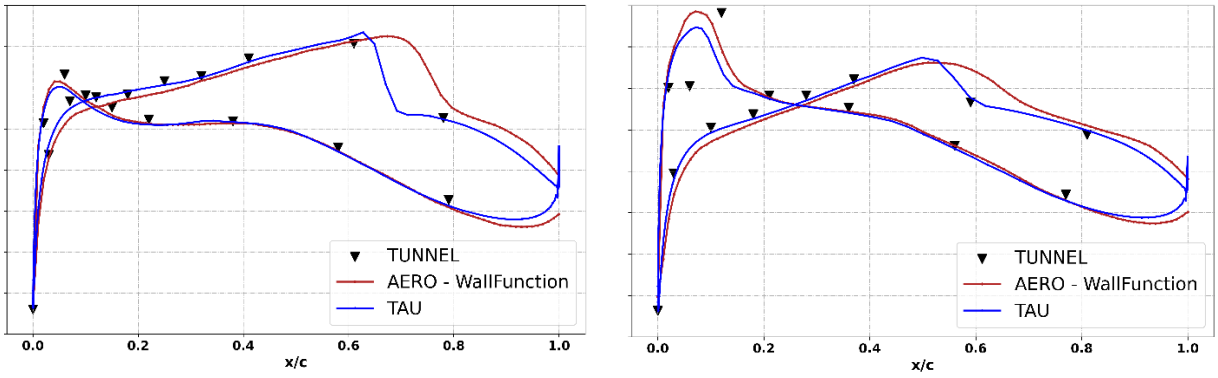

Figure 21: Comparison of simulated Cp distributions at spanwise stations η=65% (left) *and* 84% (right) - polar *HMAE-26-02-315-M82-55-SA*, Mach 0.82, alpha =0 deg, Q=55kPa.

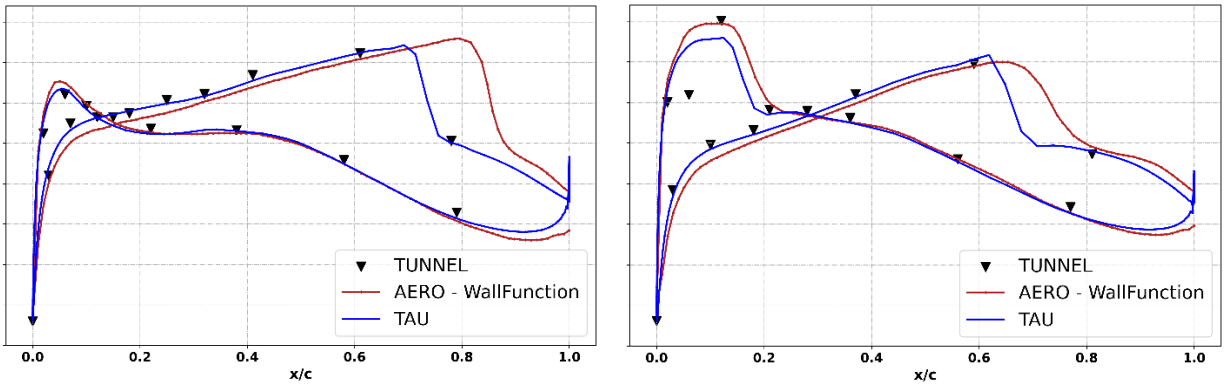

Figure 22: Comparison of simulated Cp distributions at spanwise stations η=65% (left) *and* 84% (right) - polar *HMAE-27-04-345-M84-55-SA*, Mach 0.84, alpha =0 deg, Q=55kPa.

4.2 Flutter

The wing model sensitivity to torsional loads was observed during the wind tunnel tests. Due to this characteristic, a set of tests was conducted on the dynamic FE model and on the aerodynamic DLM model, aiming to assess whether the structural or the aerodynamic parameter was the most important for flutter.

The FE model used is the same as the one created by NLR and applied at DLR (Figure 5). The Nastran aerodynamics was performed through a factorization over the WTFACT correction. It was not possible to test all the parametric conditions of interest, although some more simple parametric evaluations were simulated and presented in Figure 23 and Figure 24.

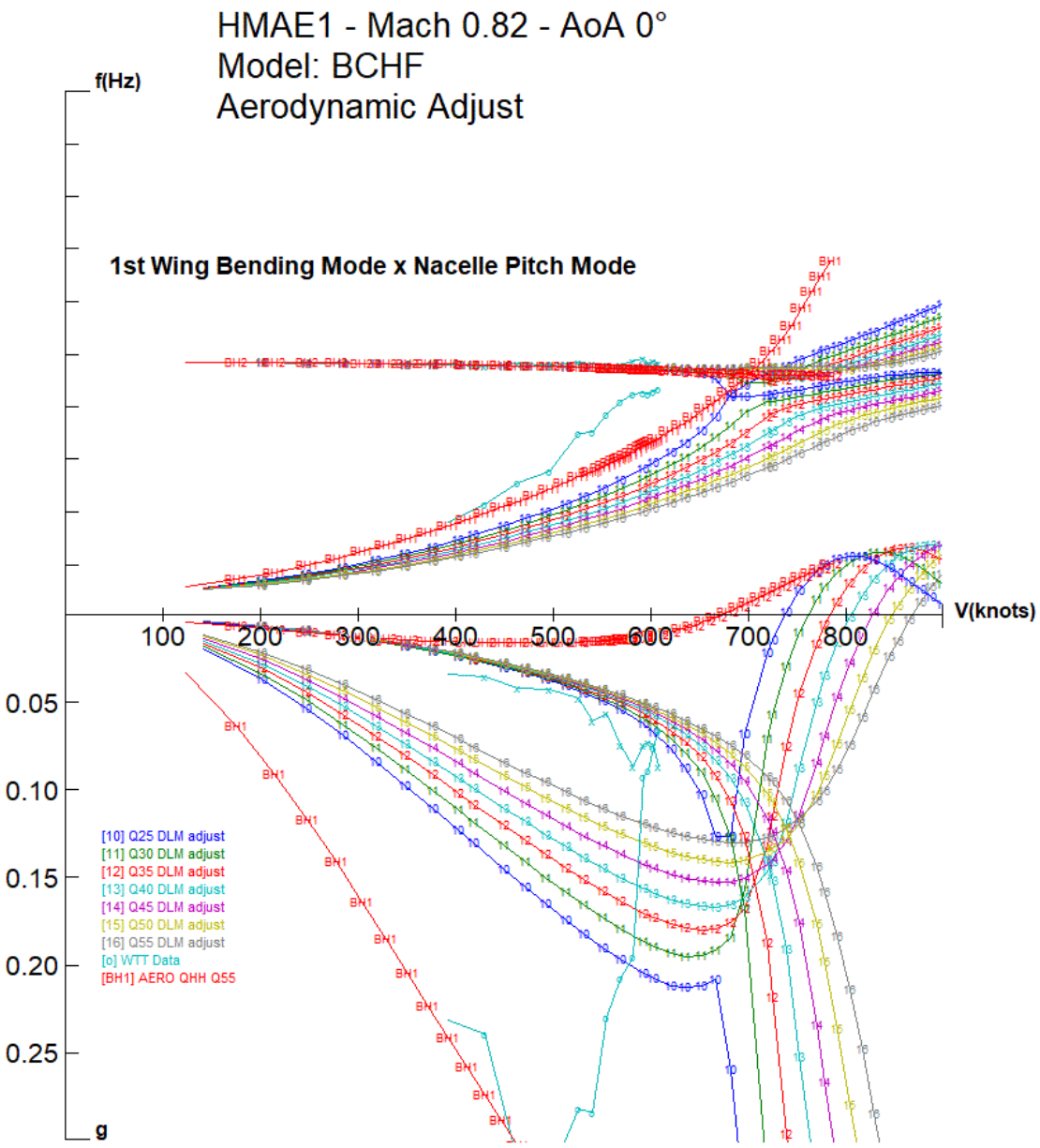

Figure 23: WTFACT variation around only one dynamic pressure adjustment at Mach 0.82.

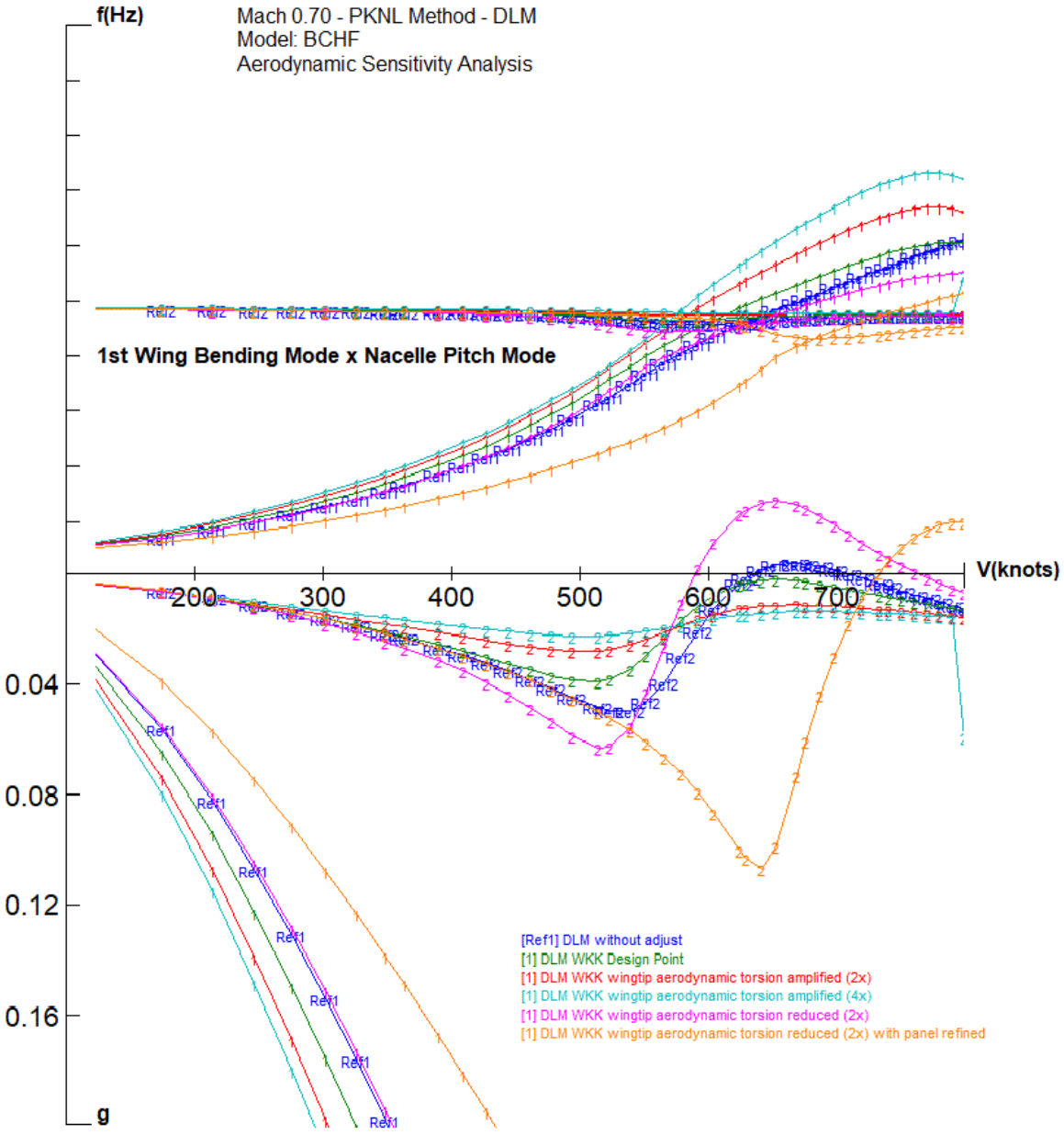

Figure 24: WTFACT variation focused on wingtip torsion at Mach 0.70.

Figure 23 shows a comparison among several adjustments considering variations of dynamic pressures using DLM and a single dynamic pressure for AERO simulation. It can be inferred that the simulation with AERO seems to be closer to the results of the wind tunnel test, while the simulations with DLM show a late coupling.

On the other hand, Figure 24 shows the tests of a forced torsion at the wingtip by modifying the aerodynamic loading on the DLM at this region. This proposal has shown the sensitivity of the aerodynamic parameter against the structural parameter.

The model can well represent the wind tunnel test and Figure 25 illustrates the flutter results at Mach 0.70. Figure 25 (a) shows in detail the second mode, while Figure 25 (b) shows for the first mode.

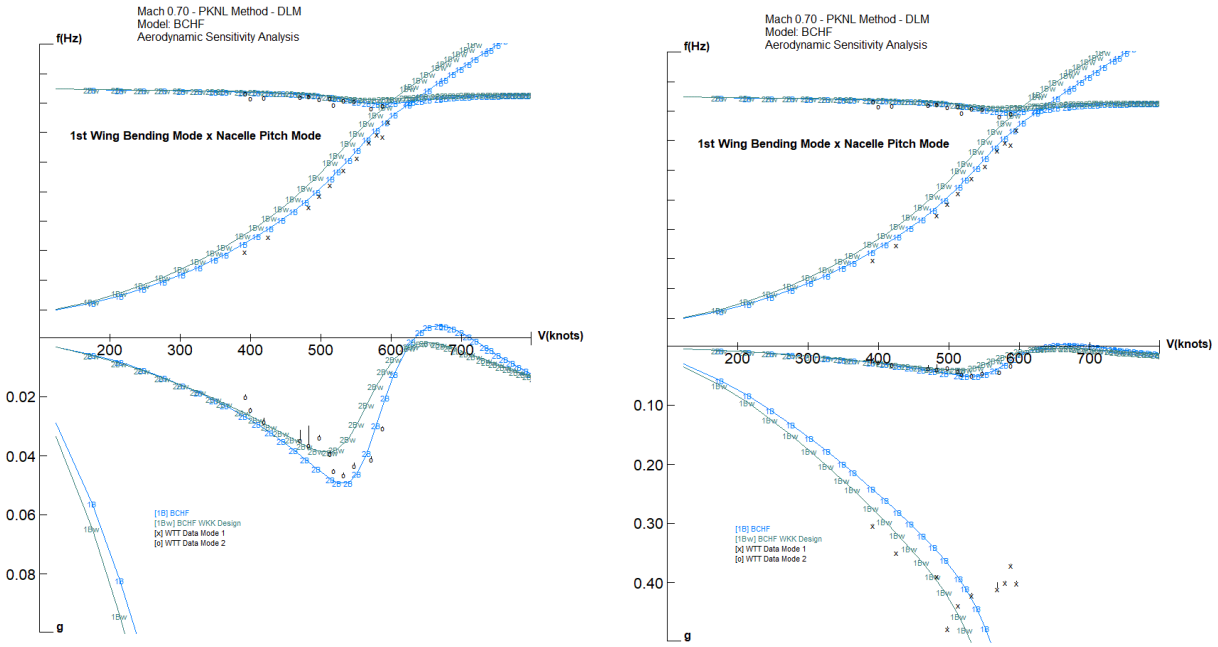

(a) (b)

Figure 25: Comparison between Nastran DLM (with and without adjustment) and Wind Tunnel Test data at Mach 0.70 in different scales for damping.

5 CONCLUSIONS

A highly flexible half-wing model was tested in transonic flow conditions in the HST wind tunnel. This model was ground tested to measure and verify its structural dynamics characteristics. Then, a wind tunnel test campaign was carried out to measure its transonic flutter behavior. The collected data included the variation of frequency and damping with the flow velocity for a few vibrational modes. Pressure coefficients were also measured during the tests.

A series of numerical simulations were conducted both by DLR and Embraer to compare the results with experimental data obtained in the wind tunnel and to evaluate the simulation tools available for such type of predictions. Embraer used the well-established DLM method and high-fidelity CMSoft AERO software. DLR, in its turn, used its in-house CFD-based TAU, which can analyze many types of aeroelastic problems, including FSI simulations.

The steady simulations showed that the pressure coefficients predicted using AERO are in good agreement with the ones from the wind tunnel measurements. For several flow conditions, and hence flight loads and shapes, the computed pressure coefficients agree reasonably well with the measured ones.

Since the wind-tunnel model is highly flexible, torsional loads influence the model geometry quite significantly and it was found that special attention must be paid to the discretization of the aerodynamics model. The flutter behavior exhibited higher sensitivity to the DLM discretization.

The use of an AERO computed QHH to feed the default Nastran SOL145 QHH showed an improvement on the results when compared to the computation with adjusted DLM matrices. Although the computations with AERO were done for only one flight shape, its results were in good agreement with experiments for most flow conditions. However, probably due to the type of modeling used for the boundary layer, some of the transonic Mach physics were only moderately captured in the simulations.

As a conclusion, it seems that the dynamic model is representative to the behavior of the flexible half wing but due to the excessive torsional flexibility, the simulations are highly sensitive to the aerodynamic modelling/configuration. The aerodynamic modelling effects are dominant in the transonic flutter behavior.

REFERENCES

[1] Govers, Y., Mai, H., Arnold, J., Dillinger, J.K.S., Pereira, A.K.A., Breviglieri Jr., C., Takara, E.K., Correa, M.S., Mello, O.A.F., Marques, R.F.A., Geurts, E.G.M., Creemers, R.J.C., Timmermans, H.S., Habing, R., Kapteijn, K. (2019) Wind tunnel flutter testing on a highly flexible wing for aeroelastic validation in the transonic regime within the HMAE1 project. In: International Forum on Aeroelasticity and Structural Dynamics 2019, IFASD 2019, IFASD. IFASD 2019 – International Forum on Aeroelasticity and Structural Dynamics, 10.-13. June 2019, Savannah, GA (USA).

[2] Timmermans, H.S., van Tongeren, J.H., Geurts, E.G.M., Marques, R.F.A., Correa, M.S., Waitz, S. (2019) Design and Validation of a Numerical High Aspect Ration Aeroelastic Wind Tunnel Model (HMAE1). In: International Forum on Aeroelasticity and Structural Dynamics 2019, IFASD 2019, IFASD. IFASD 2019 – International Forum on Aeroelasticity and Structural Dynamics, 10.-13. June 2019, Savannah, GA (USA).

[3] German-Dutch Wind Tunnels. Available in: https://www.dnw.aero/wind-tunnels/. Accessed in May, 15th 2024.

[4] Böswald, M., Govers, Y., Jelicic, G., Buchbach, R. (2019) Online Monitoring of Flutter Stability During Wind Tunnel Testing of an Elastic Wing with Pylon and Engine Nacelle within the HMAE1 Project. In: International Forum on Aeroelasticity and Structural Dynamics 2019, IFASD 2019, IFASD. IFASD 2019 – International Forum on Aeroelasticity and Structural Dynamics, 10.-13. June 2019, Savannah, GA (USA).

[5] CMSoft, Inc. Available in: https://www.cmsoftinc.com/CMS-Home/. Accessed in May, 15th 2024.

[6] Spalart, P.R.; Allmaras, S.R.: A One-Equation Turbulence Model for Aerodynamic Flows. AIAA Paper, No.92-0439, 1992.

[7] Gerhold, T.; et.al.: Calculation of Complex Three-Dimensional Configurations Employing the DLR-TAU-Code. AIAA Journal, Volume 0167, 1997.

[8] Neumann, J.; Kruger.: Coupling Strategies for Large Industrial Models. In: Notes on Numerical Fluid Mechanics and Multidisciplinary Design: Computational Flight Testing, Volume 123, Pages: 207-222 ISBN 978-3-642-38876-4, Springer, 2013.

COPYRIGHT STATEMENT

The authors confirm that they, and/or their company or organization, hold copyright on all of the original material included in this paper. The authors also confirm that they have obtained permission from the copyright holder of any third-party material included in this paper to publish it as part of their paper. The authors confirm that they give permission, or have obtained permission from the copyright holder of this paper, for the publication and public distribution of this paper as part of the IFASD 2024 proceedings or as individual off-prints from the proceedings.